Astronomical Notes

Astronomische Nachrichten

Founded by H. C. Schumacher in 1821

WILEY-VCH

The Monoceros radio loop: Temperature, brightness, spectral index, and distance

V. Borka Jovanović[1,⋆] and **D. Urošević**[2]

[1] Laboratory of Physics (010), Vinča Institute of Nuclear Sciences, P.O. Box 522, 11001 Belgrade, Serbia
[2] Department of Astronomy, Faculty of Mathematics, University of Belgrade, Studentski trg 16, 11000 Belgrade, Serbia

Received 2009 Jan 12, accepted 2009 Apr 11
Published online 2009 Jul 20

Key words radiation mechanisms: non-thermal – radio continuum: general – supernova remnants – surveys

In this paper we estimated the temperatures and brightnesses of the Monoceros radio loop at 1420, 820 and 408 MHz. The linear spectrum is estimated for mean temperatures versus frequency between 1420, 820 and 408 MHz. The spectral index of Monoceros loop is also obtained. The brightness temperatures and surface brightnesses of the loop are computed using data taken from radio-continuum surveys at the three frequencies. The spectral index of the loop is also obtained from T-T plots between 1420–820, 1420–408, and 820–408 MHz. The obtained results confirm non-thermal origin of the Monoceros radio loop.

1 Introduction

The Monoceros filamentary loop nebula was suggested to be a supernova remnant (SNR) by Davies (1963) on the basis of 237 MHz observations. This shell source of radio emission was suspected already by Davies (1963) to be a SNR, while Gebel & Shore (1972) developed this idea into a more detailed study. It was considered as an object similar to major loops when Spoelstra (1973) included it in his study of galactic loops as supernova remnants expanding in the local galactic magnetic field.

Graham et al. (1982) found that the constellation of Monoceros is remarkably rich in extended Galactic radio sources. Large parts of it have been mapped in the radio continuum over a wide range of frequencies. Monoceros Nebula can be found in a catalog of Galactic SNRs listed as G205.5+0.5 (Green 2004, 2006). It is a S-type remnant (shell remnant), characterized by a diffuse, shell-like emission with a steep radio spectrum and a size of $\sim 220'$. Shell-type supernova remnants are believed to be particle accelerators to energy up to a few hundred TeV, and it is shown that Monoceros loop is a good candidate for acceleration of particles (Fiasson et al. 2007).

The aim of this paper is to calculate the average brightness temperatures and surface brightnesses of the Monoceros radio loop at 1420, 820 and 408 MHz and to study how these results compare with previous result (Urošević & Milogradov-Turin 1998; Milogradov-Turin & Urošević 1996) and with current theories of supernova remnant evolution. These theories predict that SNRs are at radio frequencies predominantly non-thermal sources which are spreading inside of the hot and low density bubbles made by former supernova explosions or by strong stellar winds (see Salter 1983; McKee & Ostriker 1977, and references therein). The spectrum (temperature versus frequency) has been plotted and this result is used to determine the spectral index of the Monoceros loop.

2 Analysis

2.1 Data

In this paper we used observations from several radio-continuum surveys given in "Flexible Image Transport System" (FITS) format which are available on MPIfR's Survey Sampler ("Max-Planck-Institut für Radioastronomie", Bonn). This is an online service (http://www.mpifr-bonn.mpg.de/survey.html), which allows users to pick a region of the sky and obtain images and observed data (in FITS format) at a number of wavelengths. User can choose a coordinate system, projection type and a survey. The radio continuum surveys at 1420, 820 and 408 MHz provided the database for computing brightness temperatures ($T_{\rm b}$). The 1420-MHz Stockert survey (Reich & Reich 1986) has a angular resolution of $35'$, the 820-MHz Dwingeloo survey (Berkhuijsen 1972) of $1\overset{\circ}{.}2$, and the 408-MHz all-sky survey (Haslam et al. 1982) of $0\overset{\circ}{.}85$. The corresponding observations are given at the following rates for both l and b: $(1/4)^\circ$ at 1420 MHz, $(1/2)^\circ$ at 820 MHz, and $(1/3)^\circ$ at 408 MHz. The effective sensitivities for T_b are about 50 mK, 0.20 K, and about 1.0 K, respectively.

2.2 Method

We extracted observed brightness temperatures from FITS format into ASCII data files and after that, these data files

⋆ Corresponding author: vborka@vinca.rs

Table 1 Temperatures and brightnesses of Monoceros radio loop at 1420, 820, and 408 MHz.

Freq. (MHz)	Temp. Limits $T_{\rm min}$, $T_{\rm max}$ (K)	Temp. (K)	Brightness (10^{-22} W m^{-2} Hz^{-1} sr^{-1})
1420	3.8, 4.2	0.18±0.05	1.09±0.30
820	8.8, 10.7	0.90±0.20	1.85±0.40
408	36, 47	5.2±1.0	2.63±0.50

have been processed by our software, i.e. we have developed several programs in C and FORTRAN in order to obtain results presented in this paper.

The area of Monoceros loop is very difficult to determine precisely due to great influence of background radiation and superposed external sources, such as Rosette Nebula (Graham et al. 1982; Aharonian et al. 2004, 2007; Kim et al. 2007). Therefore, some authors made very rough estimates for the shape of this loop, representing it by fitted circles (see e.g. Aharonian et al. 2004; Kim et al. 2007). In order to make better estimates for the loop boundaries, we analyzed temperature profiles (see Fig. 1) for different values of Galactic latitude (b) between –6° and +6°, and for Galactic longitude (l) from 212° to 198°. As one can see in Fig. 1, there are two temperature peaks. The lower one corresponds to the total brightness temperature of the loop (including background radiation), while the higher one corresponds to superposed external sources. We denoted the minimum and maximum brightness temperature of the lower peak by $T_{\rm min}$ and $T_{\rm max}$, respectively. These temperature limits enable us to distinguish the loop from background and also from external sources, and their values are given in Table 1. Moreover, using the temperature profiles we found that the Monoceros loop is located in this sky region: $l \in [210^\circ, 200^\circ]$ and $b \in [-6^\circ, 5^\circ]$.

The area of Monoceros loop is enclosed with brightness temperature contours (see Fig. 2). These contour lines correspond to the minimum and maximum brightness temperatures which define its borders (see Table 1), and 9 contours in between. We have subtracted the background radiation, as well as the superposed radiation, in order to derive the mean brightness temperature of the SNR alone (see Borka 2007; Borka, Milogradov-Turin & Urošević 2008).

For deriving temperatures over the Monoceros loop, the areas used for the individual spurs were obtained from the radio continuum maps at three frequencies: 1420 MHz (Reich & Reich 1986), 820 MHz (Berkhuijsen 1972), and 408 MHz (Haslam et al. 1982). The areas over which an average brightness temperature is determined at each of the three frequencies are taken to be as similar as possible within the limits of measurement accuracy. Temperature limits $T_{\rm min}$ and $T_{\rm max}$, given in Table 1, are the lower and the upper temperature values: $T_{\rm min}$ is the lower temperature limit between the background and the spur, while $T_{\rm max}$ is the upper temperature limit between the spur and superposed confusing sources. In this manner, background radiation was considered as radiation that would exist if there were no spurs. If the value of $T_{\rm min}$ ($T_{\rm max}$) is changed by some small value (approximately 0.1 K for 1420 MHz and more for other frequencies), the brightness contours become significantly different. For evaluating brightness temperature of the background, we used all measured values below $T_{\rm min}$, inside the corresponding intervals of l and b, and lying on the outer side of a loop. The value of $T_{\rm b}$ is approximately constant near a loop. For evaluating the brightness temperature of a loop including the background, we used all measured values between $T_{\rm min}$ and $T_{\rm max}$ inside the corresponding regions of l and b. The mean brightness temperature for the loop is found by subtracting the mean value of background brightness temperature from the mean value of the brightness temperature over the area of the loop. From the brightness temperature we derived the surface brightness, Σ, by

$$\Sigma = (2k\nu^2/c^2)\, T_{\rm b}, \qquad (1)$$

where k is Boltzmann constant and c the speed of light. Results are given in Table 1.

The surface brightnesses of SNRs must be above the sensitivity limit of the observations and must be clearly distinguishable from the Galactic background emission (Green 1991). Therefore, the data from the fainter parts of the loops (which are very low surface brightness SNRs) are not taken into account because it is very difficult to resolve them from the background. On the other hand, this would significantly reduce brightness of entire loop and there is a general trend that fainter SNRs tend to be larger (Green 2005). For evaluation brightness temperatures over the spurs we had to take into account background radiation (Webster 1974). Borders enclosing the spurs are defined to separate the spur and its background.

The measured data have different resolutions for different frequencies (see Sect. 2.1), and therefore in order to obtain T-T plots the data are retabulated so the higher resolution maps are convolved to the resolution of the lowest resolution map. In that way we convolved data at 1420 and 408 MHz to $0.^\circ5 \times 0.^\circ5$ resolution, which is the sampling rate of the 820 MHz survey. These retabulated data are presented in Fig. 3 for the following frequencies: 1420 MHz (top left), 820 MHz (top right), 408 MHz (bottom left). Then, for each frequency pair we used only the common points (with the same (l, b)) which belong to the loop area at both frequencies (see Fig. 3, bottom right). In that way we reduced loop area to the same area for different frequencies. The obtained T-T plots for three pairs of frequencies (between 1420–820, 1420–408, and 820–408 MHz) enabled calculating the spectral indices. For each of the three frequency pairs, by interchanging the dependent and independent variables we have obtained two β values for each pair and the mean value of these fit results is adopted as the radio spectral index, as suggested in Uyaniker et al. (2004).

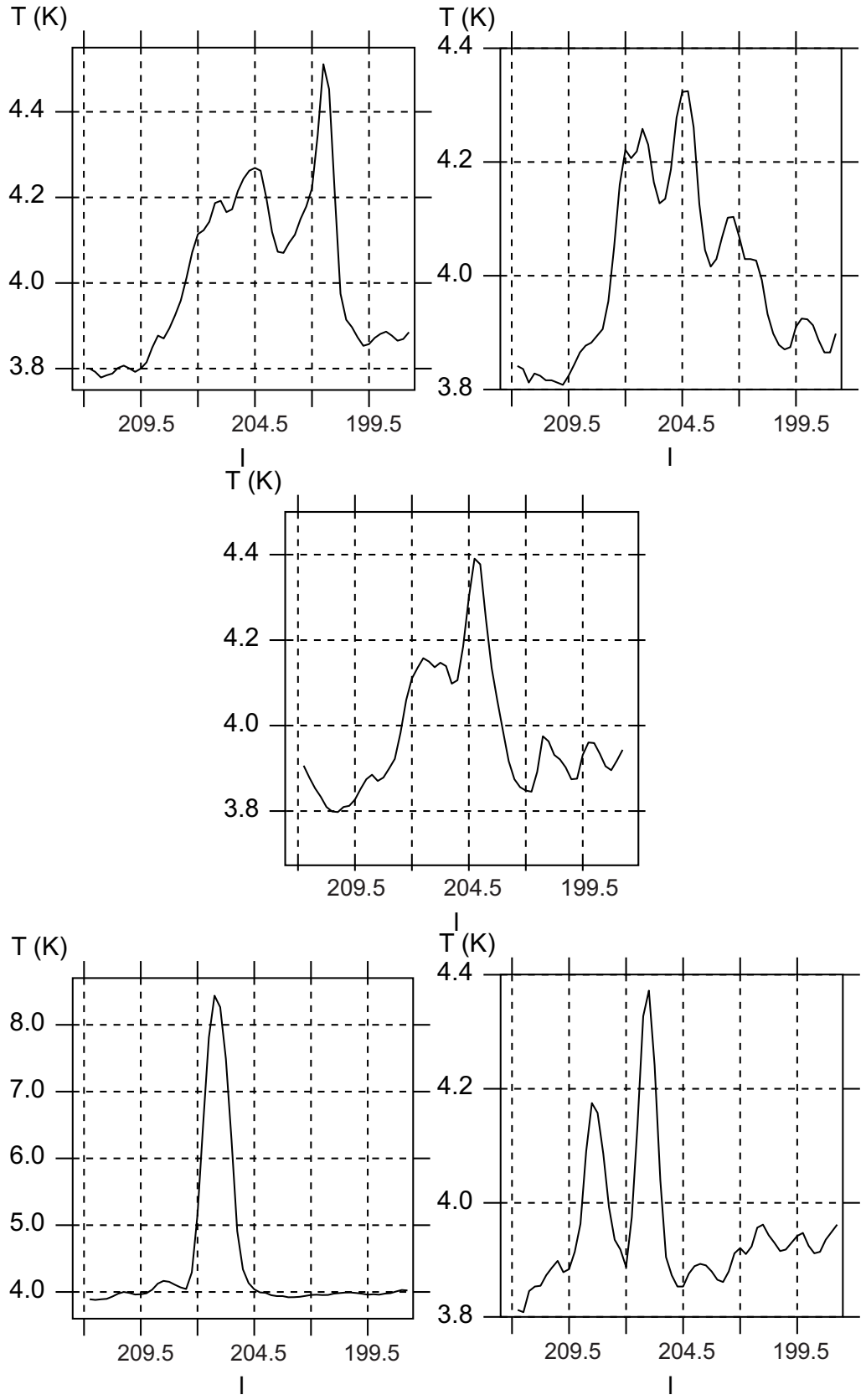

Fig. 1 Temperature profiles at 1420 MHz for Galactic longitude from 212° to 198° and for the following values of Galactic latitude: 1°.5 (*top left*), 1° (*top right*), 0° (*middle*), –2° (*bottom left*), and –3° (*bottom right*). Temperatures are given in K, and Galactic longitudes in degrees.

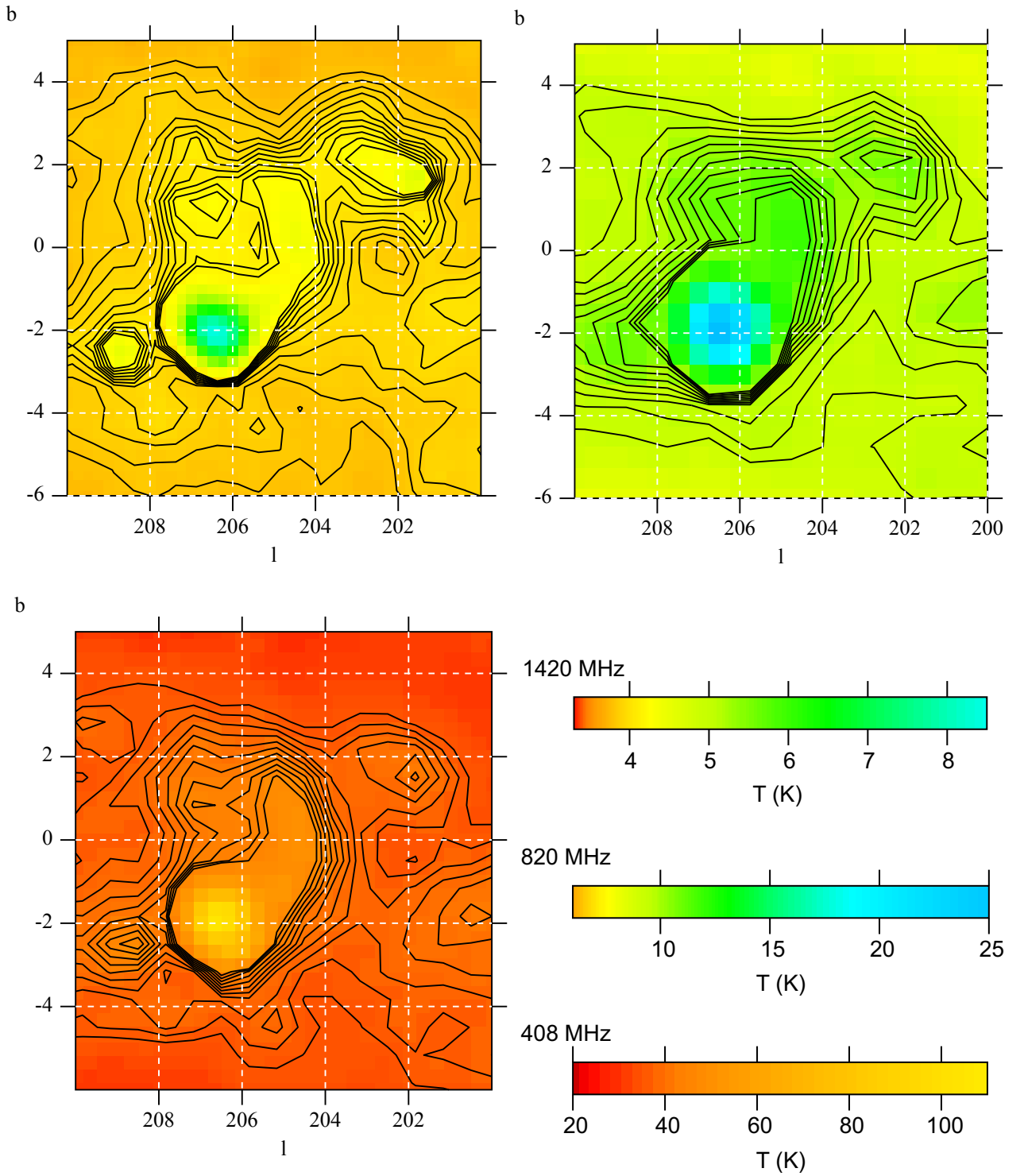

Fig. 2 (online colour at: www.an-journal.org) The map of a region in Monoceros, in new Galactic coordinates (l, b). Contours of the brightness temperatures T_b are plotted. *Top left*: the 1420 MHz map with contours of T_b given in units of K. The contours are plotted every 0.04 K, starting from the lowest temperature of 3.8 K up to 4.2 K. *Top right*: the 820 MHz map with T_b in K. The contours are plotted every 0.19 K, starting from 8.8 K up to 10.7 K. *Bottom left*: the 408 MHz map with T_b in K. The contours are plotted every 1.1 K, starting from 36 K up to 47 K. *Bottom right*: temperature colorbars for 1420, 820, and 408 MHz, all in K.

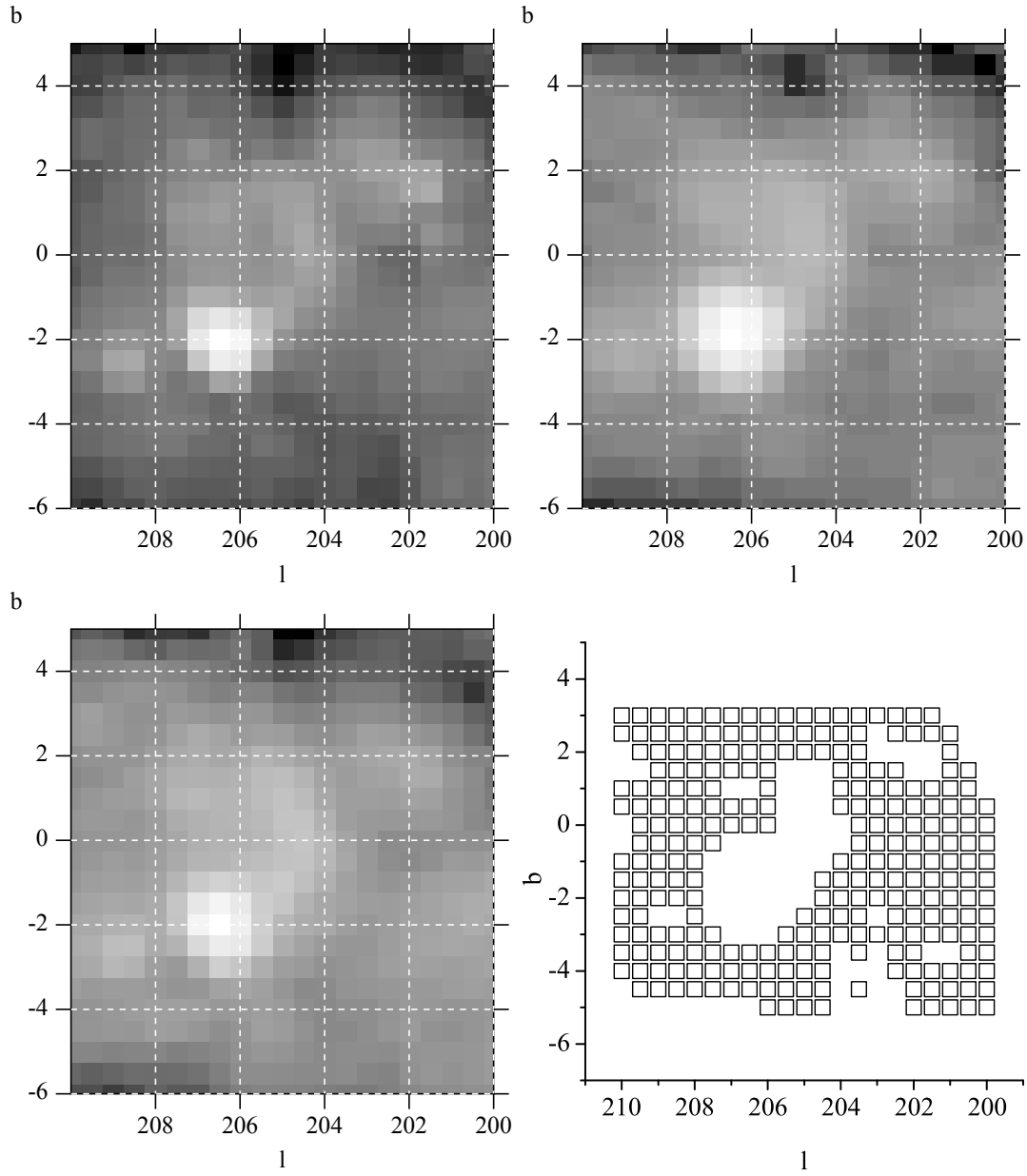

Fig. 3 The data retabulated to $0.^{\circ}5 \times 0.^{\circ}5$ resolution, for the following frequencies: 1420 MHz (*top left*), 820 MHz (*top right*), and 408 MHz (*bottom left*). *Bottom right*: the common pixels which belong to the loop area at all frequencies.

3 Results and discussion

The average brightness temperatures and surface brightnesses of Monoceros radio loop at the three frequencies are given in Table 1. The spectrum shows how temperature depends on frequency:

$$\log T = \log K - \beta \log \nu, \tag{2}$$

where K is a constant, and β is the radio spectral index.

The spectrum was generated using mean temperatures at three different frequencies. This best-fit straight line spectrum enables calculation of spectral index as negative value of the line's direction coefficient. The spectrum is shown in Fig. 4. Relative errors of the measurements, $\Delta \log T = \Delta T/(T \ln 10)$, are presented by error bars, where ΔT are the corresponding absolute errors given in Table 1. The obtained value $\beta = 2.70 \pm 0.14$ (greater than 2.2) confirms a non-thermal origin of the Monoceros loop emission. The value for the brightness temperature spectral index of the Monoceros loop is rather steep (about 2.7). This is at the high end of the spectral index distribution for SNRs as suggested in Clark & Caswell (1976).

From the relation (T-T plot)

$$T_{\nu 1}/T_{\nu 2} = (\nu_1/\nu_2)^{-\beta}, \tag{3}$$

β can be determined as

$$\beta = \log(a_{12})/\log(\nu_1/\nu_2), \tag{4}$$

where a_{12} is the direction coefficient of line $T_{\nu 2}(T_{\nu 1})$.

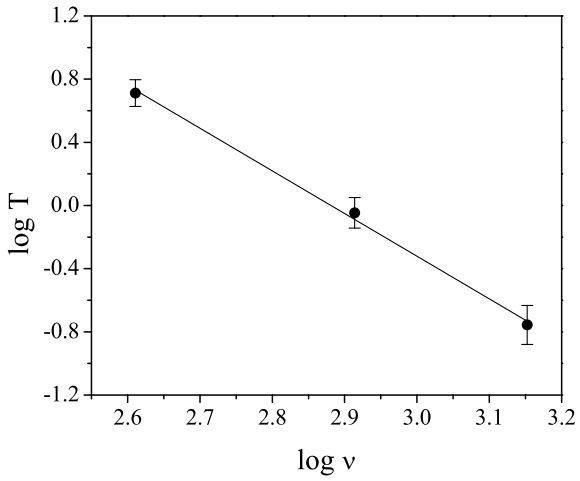

Fig. 4 Monoceros loop spectrum: temperature versus frequency, for three measurements – at 408, 820, and 1420 MHz.

Because of the influence of superposed sources to the loop and because it is hard to estimate precise loop's borders, we present how spectral indices vary for different b. Variations of spectral indices between the three frequency pairs obtained from T-T plots, distributed over Galactic latitudes, are given in Tables 2–4. For some Galactic latitudes, there is a large dispersion of the points in T-T graphs so they are not suitable for calculation of spectral index; we did not calculate β for them, indicated in the tables by "-". The averaged values of the radio spectral indices are given in Table 5. Examples of T-T plots between 1420–820, 1420–408, and 820–408 MHz for longitude $b = 1°$ are given in Fig. 5. The average value of the spectral index from T-T is $\langle\beta_{TT}\rangle = 2.63 \pm 0.30$. It can be noticed that this value agrees well with the corresponding value obtained from spectrum, as expected (see Uyaniker et al. 2004). Then we calculated the mean value of the spectral index between 1420, 820, and 408 MHz (regarding the spectrum and T-T graphs) to $\langle\beta\rangle = 2.66 \pm 0.20$. With this $\langle\beta\rangle$ we reduced Σ_ν to 1000 MHz (Table 6) according to the relation

$$\Sigma_{1\mathrm{GHz}}/\Sigma_{\nu\mathrm{GHz}} = (\nu/1)^{(\beta-2)}. \quad (5)$$

In Graham et al. (1982), the value $\beta = 2.47 \pm 0.06$ of radio spectral index of this loop was derived from the radio continuum spectrum between two frequencies: 111 and 2700 MHz, and we calculated a spectrum using three frequencies and also derived T-T graphs which represent a different method.

Distances to the SNRs can be inferred from positional coincidences with H I, H II regions and molecular clouds, OB associations, or pulsars or from measuring optical velocities and proper motions. Where there is no direct distance determination, estimates can be made for shell remnants by utilizing the radio surface brightness-to-diameter relationship Σ-D (Case & Bhattacharya 1998, and references therein). The mean surface brightness at a specific radio frequency, Σ_ν, is a distance-independent parameter and, to a first approximation, is an intrinsic property of the SNR (Shklovskii 1960).

Table 2 Variations of spectral indices between 1420 and 820 MHz obtained from T-T plots, distributed over Galactic latitudes.

Latitude (°)	β(1420–820)	β(820–1420)
–5.0	-	-
–4.5	-	-
–4.0	-	-
–3.5	-	-
–3.0	1.92 ± 0.82	4.54 ± 0.82
–2.5	3.86 ± 0.46	4.84 ± 0.46
–2.0	3.47 ± 0.31	4.07 ± 0.31
–1.5	2.96 ± 0.73	5.02 ± 0.73
–1.0	1.96 ± 0.55	3.31 ± 0.55
–0.5	2.61 ± 0.39	3.36 ± 0.39
0	2.39 ± 0.22	2.73 ± 0.22
0.5	2.49 ± 0.28	3.09 ± 0.28
1.0	2.42 ± 0.26	2.85 ± 0.26
1.5	2.74 ± 0.27	3.13 ± 0.27
2.0	2.62 ± 0.26	3.02 ± 0.26
2.5	1.59 ± 0.41	2.69 ± 0.41
3.0	1.26 ± 0.43	2.41 ± 0.43

Table 3 Variations of spectral indices between 1420 and 408 MHz obtained from T-T plots, distributed over Galactic latitudes.

Latitude (°)	β(1420–408)	β(408–1420)
–5.0	1.92 ± 0.24	2.32 ± 0.24
–4.5	2.14 ± 0.33	3.15 ± 0.33
–4.0	2.35 ± 0.12	2.62 ± 0.12
–3.5	-	-
–3.0	2.48 ± 0.19	3.03 ± 0.19
–2.5	2.91 ± 0.13	3.14 ± 0.13
–2.0	2.58 ± 0.11	2.78 ± 0.11
–1.5	2.55 ± 0.14	2.82 ± 0.14
–1.0	2.55 ± 0.08	2.65 ± 0.08
–0.5	2.69 ± 0.07	2.76 ± 0.07
0	2.58 ± 0.10	2.75 ± 0.10
0.5	2.39 ± 0.16	2.78 ± 0.16
1.0	2.40 ± 0.19	2.82 ± 0.19
1.5	2.16 ± 0.22	2.65 ± 0.22
2.0	2.19 ± 0.25	2.80 ± 0.25
2.5	-	3.23 ± 0.89
3.0	-	-

Using a set of 172 SNRs as calibrators, for which reliable distance values were determined, Urošević (2002) has constructed the following relation between the surface brightness (Σ) and diameter (D):

$$\Sigma_{1\mathrm{GHz}} = 2.76 \times 10^{-16} D^{-3.02}. \quad (6)$$

This relation, combining the Galactic and extragalactic SNRs (master relation), also includes four main Galactic radio loops (Loops I–IV).

It is shown (Odegard 1986) that there is diffuse emission with the filaments located in the western half of Monoceros loop (overlapping with Rosette Nebula) and in the eastern part (dust cloud L1631). There is also a peak in the 2700 MHz emission in the eastern edge for which Graham et al. (1982) suggested to be a H II region. In Aharonian et al.

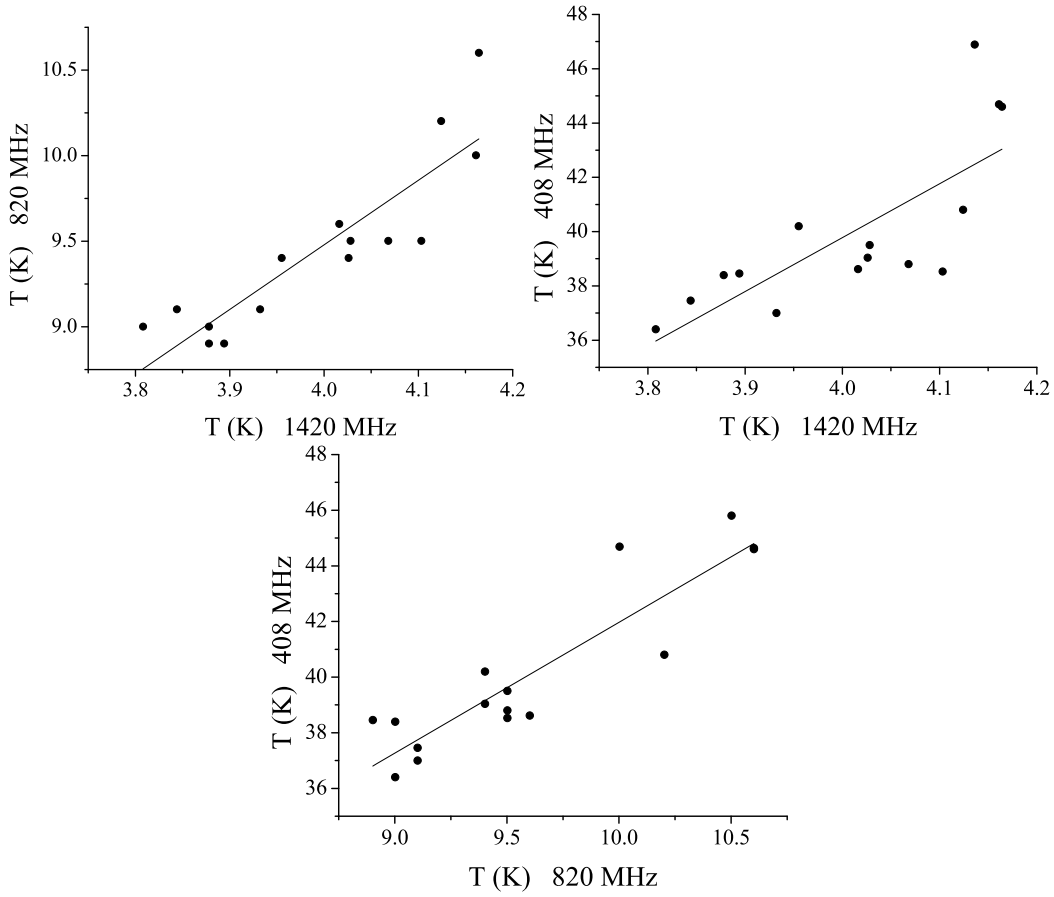

Fig. 5 *Top left*: T-T plot between 1420 and 820 MHz for the Monoceros loop at latitude $b = 1°$, in the longitude range [210°, 200°]. *Top right*: the same as top left, but between 1420 and 408 MHz. *Bottom*: the same as top left, but between 820 and 408 MHz.

(2007) it is said that the complex Monoceros loop/Rosette Nebula region contains several potential sources of very-high-energy γ ray emission and that the interaction of the SNR with a compact molecular cloud is possible. Because of possible influence with molecular clouds and H II region, we also take the Σ-D relation from Arbutina et al. (2004) adjusted for molecular clouds:

$$\Sigma_{1\mathrm{GHz}} = 1.1 \times 10^{-15} D^{-3.5}. \quad (7)$$

They have taken 14 shell-type Galactic SNRs associated with large molecular clouds.

Table 4 Variations of spectral indices between 820 and 408 MHz obtained from T-T plots, distributed over Galactic latitudes.

Latitude (°)	β(820–408)	β(408–820)
–5.0	2.38 ± 0.51	3.29 ± 0.51
–4.5	1.39 ± 0.89	4.20 ± 0.89
–4.0	1.71 ± 0.49	3.22 ± 0.49
–3.5	1.12 ± 0.56	2.74 ± 0.56
–3.0	1.87 ± 0.33	2.74 ± 0.33
–2.5	1.57 ± 0.28	2.07 ± 0.28
–2.0	1.47 ± 0.25	1.95 ± 0.25
–1.5	1.24 ± 0.35	2.07 ± 0.35
–1.0	2.23 ± 0.31	2.87 ± 0.31
–0.5	2.44 ± 0.17	2.67 ± 0.17
0	2.49 ± 0.10	2.58 ± 0.10
0.5	2.23 ± 0.12	2.36 ± 0.12
1.0	2.22 ± 0.18	2.50 ± 0.18
1.5	1.91 ± 0.25	2.36 ± 0.25
2.0	1.96 ± 0.18	2.29 ± 0.18
2.5	-	3.21 ± 0.72
3.0	-	-

Table 5 The average radio spectral indices between 1420, 820, and 408 MHz obtained from T-T plots.

Frequency Pair (MHz)	β_{TT}
1420–820	2.98 ± 0.40
1420–408	2.62 ± 0.20
820–408	2.29 ± 0.34

Table 6 Brightnesses of Monoceros radio loop reduced to 1000 MHz using $\beta = 2.66 \pm 0.20$.

Frequency (MHz)	Brightness at 1000 MHz (10^{-22} W m^{-2} Hz^{-1} sr^{-1})
1420	1.37 ± 0.50
820	1.63 ± 0.30
408	1.45 ± 0.03

Table 7 Diameters D and distances r of Monoceros radio loop derived from the Σ-D relation given by Urošević (2002) and by Arbutina et al. (2004).

Relation	D (pc)	r (pc)
(6)	119 ± 18	1630 ± 250
(7)	92 ± 14	1250 ± 190

Using the relations derived by Urošević (2002) and Arbutina et al. (2004), we computed the diameter of the loop and then the distance as

$$r = D/(2 \sin \Theta), \quad (8)$$

with angular radius Θ taken from Urošević & Milogradov-Turin (1998). The results are given in Table 7.

It can be noticed that there is the influence of molecular cloud on Monoceros loop (Graham et al. 1982; Aharonian et al. 2007). If that influence constantly existed during the loop's evolution, then for distance calculation it is more suitable Σ-D relation by Arbutina et al. (2004). If not, then it is more suitable to use relation by Urošević (2002).

For the distance to this loop, the mean optical velocity suggests 0.8 kpc, and the low frequency radio absorption suggests 1.6 kpc (Graham et al. 1982; Odegard 1986; Green 2006). With our calculated radio spectral index $\beta = 2.66 \pm 0.20$, we calculated distance to this loop using our derived brightnesses. The results are also given in Table 7.

4 Conclusions

In this paper we calculated the brightness temperatures and surface brightnesses of the Monoceros radio loop at 1420, 820, and 408 MHz. The linear spectrum is estimated for mean temperatures versus frequency between 1420, 820, and 408 MHz. It is the first time that the brightness temperatures of the Monoceros loop are calculated at 820 and 408 MHz frequencies from the observational data. We sampled much more points (more than 1000) at 1420 MHz than in previous papers (95 points) (Urošević & Milogradov-Turin 1998; Milogradov-Turin & Urošević 1996). Also, the brightness temperature is now derived using a different method. The temperature of this radio loop at 1420 MHz is in good agreement with the result obtained in Urošević & Milogradov-Turin (1998).

We present the radio continuum spectrum of the Monoceros loop using average brightness temperatures at three different frequencies. As it can be seen from Fig. 4, the given linear fit provides a reliable spectral index. Also, we present the T-T plots which enables also calculation of spectral index.

The effective sensitivity of the brightness temperatures are: 50 mK for 1420 MHz, 0.2 K for 820 MHz, and about 1.0 K for 408 MHz. The most precise measurements (the least relative errors) are in case of 1420 MHz, so positions of the brightness temperature contours of the loop are the most realistic for this frequency. The brightnesses of the Monoceros loop at 1420 and 820 and 408 MHz are in good agreement when reduced to 1 GHz.

With our derived brightnesses, we calculated new diameters and distances to this loop at the three frequencies: 1420, 820 and 408 MHz and then estimated some average distance. We used empirical Σ-D relations for supernova remnants by Urošević (2002) and Arbutina et al. (2004). The estimated distance of the Monoceros radio loop is in good agreement with the earlier results: 1.6 kpc (Guseinov et al. 2004; Green 2006).

The spectral index analysis confirms the non-thermal origin of the Monoceros radio loop.

Acknowledgements. This research is part of the projects "Gaseous and stellar component of galaxies: interaction and evolution" (No. 146012) and "Physics and chemistry with ion beams" (No. 451-01-00049) supported by the Ministry of Science of the Republic of Serbia.

References

Aharonian, F.A., et al. (HEGRA collaboration): 2004, A&A 417, 973
Aharonian, F.A., et al. (HESS collaboration): 2007, A&A 469, L1
Arbutina, B., Urošević, D., Stanković, M., Tešić, Lj.: 2004, MNRAS 350, 346
Berkhuijsen, E.M.: 1972, A&AS 5, 263
Borka, V.: 2007, MNRAS 376, 634
Borka, V., Milogradov-Turin, J., Urošević, D.: 2008, AN 329, 397
Case, G.L., Bhattacharya, D.: 1998, ApJ 504, 761
Clark, D.H., Caswell, J.L.: 1976, MNRAS 174, 267
Davies, R.D.: 1963, Obs 83, 172
Fiasson, A., Hinton, J.A., Gallant, Y., Marcowith, A., Reimer, O., Rowell, G. (for the H.E.S.S. Collaboration): 2007, arXiv: astro-ph/0709.2550
Gebel, W.L., Shore, S.N.: 1972, ApJ 172, L9
Graham, D.A., Haslam, C.G.T., Salter, C.J., Wilson, W.E.: 1982, A&A 109, 145
Green, D.A.: 1991, PASP 103, 209
Green, D.A.: 2004, BASI 32, 335
Green, D.A.: 2005, MmSAI 76, 534
Green, D. A.: 2006, A Catalogue of Galactic Supernova Remnants (2006 April version), Cavendish Laboratory, Cambridge, UK.
Guseinov, O.H., Ankay, A., Tagieva, S.O.: 2004, Serb. Astron. J. 168, 55
Haslam, C.G.T., Salter, C.J., Stoffel, H., Wilson, W.E.: 1982, A&AS 47, 1
Kim, I.-J., Min, K.-W., Seon, K.-I., et al.: 2007, ApJ 665, L139
McKee, C.F., Ostriker, J.P.: 1977, ApJ 218, 148
Milogradov-Turin, J., Urošević, D.: 1996, Publ. Astron. Obs. Belgrade 54, 47
Odegard, N.: 1986, ApJ 301, 813
Reich, P., Reich, W.: 1986, A&AS 63, 205
Salter, C.J.: 1983, BASI 11, 1
Shklovskii, I.S.: 1960, SvA 4, 243
Spoelstra, T.A.Th.: 1973, A&A 24, 149
Urošević, D.: 2002, Serb. Astron. J. 165, 27
Urošević, D., Milogradov-Turin, J.: 1998, Serb. Astron. J. 157, 35
Uyaniker, B., Reich, W., Yar, A., Furst, E.: 2004, A&A 426, 909
Webster, A.S.: 1974, MNRAS 166, 355

